Single-shot areal profilometry using hyperspectral interferometry with a microlens array

PABLO D. RUIZ* AND JONATHAN M. HUNTLEY

Wolfson School of Mechanical, Electrical and Manufacturing Engineering, Loughborough University, Loughborough, UK, LE11 3TU

**p.d.ruiz@lboro.ac.uk*

Abstract: We describe a single-shot technique to measure areal profiles on optically smooth and stepped surfaces for applications where rapid data acquisition in non-cooperative environments is essential. It is based on hyperspectral interferometry (HSI), a technique in which the output of a white-light interferometer provides the input to a hyperspectral imaging system. Previous HSI implementations suffered from inefficient utilisation of the available pixels which limited the number of measured coordinates and/or unambiguous depth range. In the current paper a >20-fold increase in pixel utilisation is achieved through the use of a 2-D microlens array, that leads to a 35×35 channel system with an unambiguous depth range of 0.88 mm.

OCIS codes: (120.3180) Interferometry; (120.2830) Height Measurements; (120.3940) Metrology.

References and links

1. L. Deck, and P. de Groot, "High-speed noncontact profiler based on scanning white-light interferometry,"Appl. Opt. **33**, 7334-7338 (1994).
2. P. Sandoz, and G. Tribillon, "Profilometry by zero-order interference fringe identification,"J. Mod. Opt. **40**, 1691-1700 (1993).
3. T. Dresel, G. Häusler, and H. Venzke, "Three-dimensional sensing of rough surfaces by coherence radar," Appl. Opt. **31**, 919-925 (1992).
4. S. Kuwamura, and I. Yamaguchi, "Wavelength scanning profilometry for real-time surface shape measurement,"Appl. Opt. **36**, 4473-4482 (1997).
5. M. Takeda and H. Yamamoto, "Fourier-transform speckle profilometry: Three-dimensional shape measurement of diffuse objects with large height steps and/or spatially isolated surfaces,"Appl. Opt. **33**, 7829-7837 (1994).
6. J. M. Huntley, T. Widjanarko, and P. D. Ruiz, "Hyperspectral interferometry for single-shot absolute measurement of two-dimensional optical path distributions,"Meas. Sci. Tech. **21**, 075304 (2010).
7. T. Widjanarko, J. M. Huntley, and P. D. Ruiz, "Single-shot profilometry of rough surfaces using hyperspectral interferometry,"Opt. Lett. **37**, 350-352 (2012).
8. R. Bacon et. al., "3d spectrography at high spatial resolution. I. Concept and realization of the integral field spectrograph tiger,"Astronomy and Astrophysics Supplement Series, **113**, 347-357 (1995).
9. M. Shepherd, "Correct sampling of diffraction limited images," (California Institute of Technology, CCAT-p, 2012). Technical Memo. http://wiki.astro.cornell.edu/twiki/pub/CCAT/CCAT_Memos/DiffractionLimitedSampling111212.pdf
10. J. M. Huntley, "An image processing system for the analysis of speckle photographs,"J. Phys. E: Scientific Instruments **19**, 43-49 (1986).

1. Introduction

White light interferometry (WLI) is an effective technique to measure absolute distance and surface profile of components with steep slopes, for example due to geometrical discontinuities or surface roughness. The use of multiple wavelengths eliminates the need for phase unwrapping and hence the height measurement errors that can occur with a monochromatic source.

There are at least three approaches to implement WLI. The first, on which many commercial profilometers are based, is known as scanning white light interferometry (SWLI) [1-3]. In this type of interferometer the object or Mirau imaging lens is moved while keeping

the reference beam stationary, and the point of maximum fringe modulation is detected and recorded on a pixelwise basis. In the second approach, known as wavelength (or frequency) scanning interferometry (WSI or FSI), both interferometer arms remain fixed and the wavelength is scanned over time [4, 5]. The scanning nature of these two approaches imposes significant environmental stability requirements as the interferometer and sample must remain stationary with respect to each other to within a small fraction of the wavelength during the acquisition of typically hundreds of interferograms.

A third approach that eliminates any sort of scanning was recently proposed to measure a surface profile with single-shot image acquisition, thus minimizing the effects of environmental disturbance. Known as hyperspectral interferometry (HSI), it is based on the combination of an interferometer and a hyperspectral imaging system [6, 7]. HSI uses a hyperspectral imager to spatially separate a set of narrowband interferograms from a single white-light interferogram. Unambiguous measurement of two-dimensional (2-D) optical path distributions can thus be obtained in a single shot. The 2-D nature of the measurements distinguishes the technique from spectral optical coherence tomography, which provides only one dimensional (1-D) distributions, i.e. 'slices' through the surface.

Prototype HSI systems and sample profiles from both optically smooth and rough surfaces have been reported in [6] and [7], respectively. A white-light image of the sample was recombined with a reference beam at the entrance of an imaging spectrometer which spread the image along a spectral axis by means of a diffraction grating. Spectral overlap was eliminated by using an etalon filter to produce a frequency comb and thus to place a sequence of quasi-monochromatic images of the object along one axis of a 2-D photodetector array. This arrangement, however, is inefficient in its use of the image sensor pixels as the grating can only disperse the broadband input of the spectrometer along one direction. The total of 62 images, each of 11×19 pixels, meant that only ~2% of the pixels in the photodetector array were used, which limits significantly the number of points in the height maps and the unambiguous depth range.

In this paper, an alternative way to spatially separate the spectral information onto the photodetector array is presented. This is based on a microlens array integral field unit (IFU) developed in astronomy for spectral imaging applications [8], and can lead to a pixel usage of over 40%, i.e. a 20× improvement on previous HSI setups.

The paper is organised as follows. The overall concept is described in Section 2, with key design parameters discussed in Section 3. Data analysis of the interferograms is covered in Section 4, experimental results from two samples presented in Section 5, and conclusions in Section 6.

2. Optical setup

2.1 Interferometer

The system consists of a Linnik-type imaging interferometer and a hyperspectral imager (left and right hand sides of Fig. 1, respectively). A super-luminescent light emitting diode, SLD, is used as the light source (Superlum Diodes Ltd, 840 HP1; 15 mW output power; centre wavelength λ_c = 840 nm; bandwidth $\Delta\lambda$ = 50 nm). Two different configurations are used to launch light into the interferometer, as shown schematically in the top left of Fig. 1 and described below.

1) 'Two wavelengths' illumination. In this configuration, the output of the SLD is connected to fibre (1) of a 2×2, 90:10 fibre coupler. Fibre (3) of the coupler is connected to a single mode fibre with two fibre Bragg gratings FBG_1 and FBG_2 which act as spectrally selective mirrors for wavelengths λ_1 = 820 nm and λ_2 = 853 nm with a narrow spectral bandwidth (<0.01 nm). Light reflected at FBG_1 and FBG_2 is delivered to the interferometer via fibre (2) of the fibre coupler. This configuration is used to calibrate the wavelength axis in the spectral images described in Section 5.

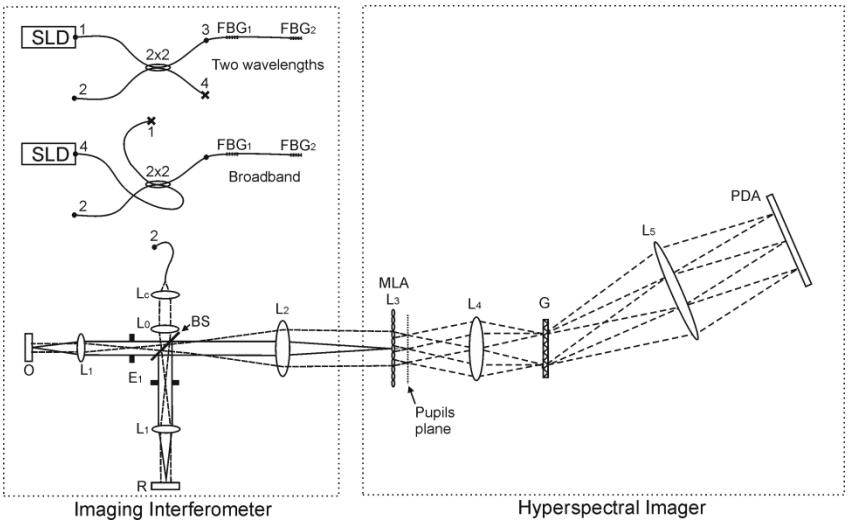

Fig. 1. Optical setup of the Hyperspectral Interferometry system based on a microlens array, showing: SLD: Super-luminescent light emitting diode; FBG_1, FBG_2: Fibre Bragg gratings; L_c: collimator; BS: beam splitter; O: object; R: reference mirror; L_0, L_1, L_2, L_4 and L_5: NIR achromatic lenses; E_1: aperture stop; MLA: microlens array; L_3: lenslet; G: diffraction grating and PDA: photodetector array. At the top of the imaging interferometer box, the 'two wavelengths' and 'broadband' illumination configurations are shown.

2) 'Broadband' illumination. In this configuration, fibre (4) of the fibre coupler is connected to the output of the SLD source, bypassing the fibre Bragg gratings and delivering broadband light directly to the interferometer via fibre (2) of the fibre coupler, as in the two wavelengths configuration.

At the interferometer's input, collimator L_c, lens L_0 and beam splitter BS produce a pair of point sources at a distance f_0 from L_0, one on each arm of the interferometer. The point sources are at the back focal planes of lenses L_1, which collimate the beam onto the reference mirror and the object. Doubly telecentric systems formed by lenses L_1 (at both reference and object arms) and L_2 image the reference mirror and the object at the back focal plane of L_2. At that plane, an image of the object is recombined with a collimated reference beam so as to form a broadband interferogram.

2.2 Spectrometer

The output of the interferometer, i.e. the image of the object recombined with the reference beam, acts as the input for a hyperspectral imager. At the image plane, a microlens array, MLA, spatially samples the image of the object (Suss MicroOptics, fused silica refractive index n_r = 1.4525 at 840 nm, lenslet diameter 100 μm, arranged on a square grid of pitch 100 μm, regions between lenses chrome-coated, radius of curvature ROC = 60 μm, effective focal length f = ROC/(n_r-1) = 130 μm, numerical aperture NA = 0.38, array size = 5×5×1.2 mm^3). A given lenslet labelled by indices (m, n) collects light from a small region on the sample surface, centred on the point with coordinates (x_m, y_n), where m = 0,1,2,...,N_x – 1, n = 0,1,2,...,N_y – 1, and N_x, N_y are respectively the number of lenslets along the x and y axes.

At the back focal plane of each lenslet (the pupil plane) a diffraction pattern is formed. When a flat wavefront is incident on the lenslet, the diffraction pattern corresponds to the point spread function (PSF) of the lenslet. The resulting array of pupils is imaged with a doubly telecentric system formed by lenses L_4 and L_5 onto a large format photodetector array,

PDA (Apogee U16M: 4096×4096 pixels, pixel size 9 μm, array size 36.86 mm, array diagonal 52.13 mm). At the pupil plane of this telecentric system a transmission, near-infrared diffraction grating G (300 lines mm^{-1}) diffracts the collimated beams produced by L_4 from each lenslet PSF. The first diffracted order is collected by lens L_5 so that the spots at the back focal plane of the MLA become lines in the plane of the PDA.

2.3 Spatial encoding of spectral information

Figure 2(a) shows a schematic view of an object that has a surface step and which is imaged onto the MLA (Fig. 2(b)). Both the coordinate system of the sample, and the row/column axes of the MLA, are rotated by a small angle α with respect to the row/column axes of the PDA. This avoids overlapping of the spectra on the PDA and allows more sample points per spectrum for a given number of MLA lenslets, as compared to the case $\alpha = 0$. A MLA with reduced number of lenses ($N_x = N_y = 5$) is used in Fig. 2(b) to illustrate the concept.

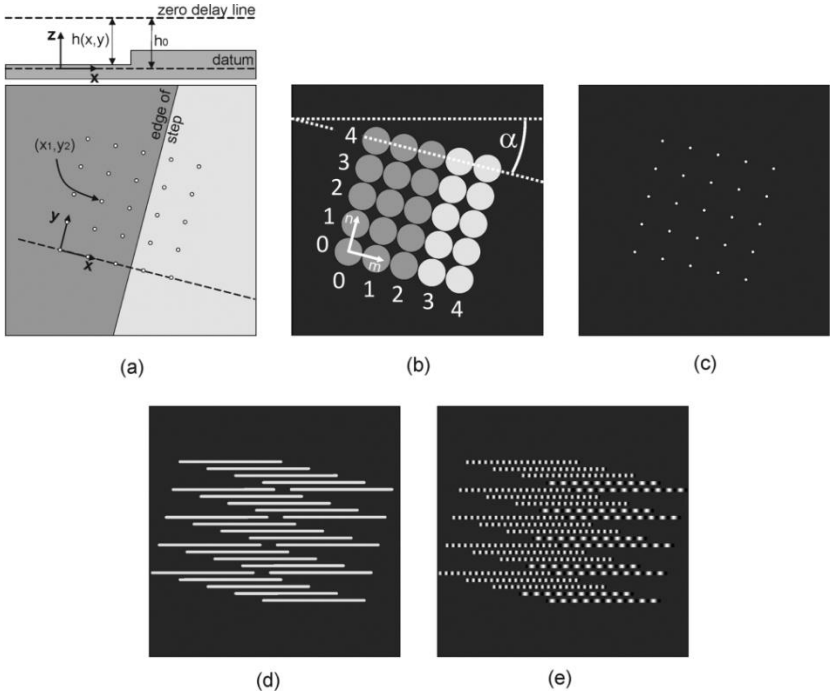

Fig. 2. Encoding of surface height in Hyperspectral Interferometry: a) object with a surface step profile. The insert above shows a cross-section through the sample with height distribution $h(x, y)$. Lines indicating cross-sections through the zero optical path difference and sample datum surfaces are also shown; b) image of the object on the microlens array; c) microlens array pupils' plane; d) array of spectra (no reference beam in the interferometer); e) spectra (shown here in monochrome for clarity) are modulated by fringes which frequency encode surface height from datum.

Figure 2(c) shows the pupil plane of the MLA. In the case of a flat wavefront reaching the MLA, we see an array of spots the shapes of which correspond to the PSFs of the lenslets. The diffraction grating G in Fig. 1 is set with the grooves parallel to the columns of the PDA array, so that the spectra align parallel to the rows. Figure 2(d) illustrates the spectra when only one of the reference or object beams is imaged onto the MLA. When both beams are present on the MLA, the spectra are modulated with fringes (see Fig. 2(e)) with a spatial frequency that encodes the optical path difference between the object and reference beams for

the corresponding lenslet in the MLA. The pixels in the row of the PDA corresponding to MLA lenslet (m, n) sample the interference signal from point (x_m, y_n) on the sample. We denote the sampling points along the wavenumber axis by k_p where p = 0, 1, 2,..., N_k – 1, and N_k is the total number of sample points. Strictly speaking there should be two additional subscripts m, n on k_p because, unlike the etalon-based system described in [6], the positions of the sample points along the k axis vary from one lenslet to another. However this variation introduces only an additional variable phase term in the depth reconstruction and does not alter the position of the Fourier-domain peak so can be neglected for depth measurement applications. To a first approximation the wavenumber sampling can be considered uniform, with a spacing of δk between adjacent pixels; there are however significant nonlinearities which need to be accounted for in order to obtain optimal depth resolution.

All the sampled spectra in Fig. 2(e) can be arranged to form a $I(x_m, y_n, k_{m,n,p})$ data cube ready for data reduction as described in section 5. Despite the differences in optical setup between the current MLA system and the etalon-based system described in [6], the fact that both result in equivalent 3-D intensity distributions (apart from the unimportant spatially-varying k-axis shift mentioned above) means that all the theoretical derivations in [6] are directly applicable here. In particular, the range of optical path difference, z, that can be unambiguously measured from the interference signal is

$$0 \le z \le z_M, \tag{1}$$

where

$$z_M = \frac{\pi}{\delta k}, \tag{2}$$

and where δk is the difference in wavenumber between successive samples. The optical path difference resolution (defined here as the distance between zero crossing points on either side of the Fourier-domain signal peak) is

$$\delta z = \gamma \frac{2\pi}{N_k \delta k}, \tag{3}$$

where γ is a constant to take account of the shape of the spectral envelope or window function applied to the data, taking for example the value 2 for a rectangular window, and 4 for a Hanning window.

When such an interferometer is applied to the measurement of a 2-dimensional height distribution $h(x, y)$, the optical path difference is

$$z = 2\left[h_0 - h(x, y)\right], \tag{4}$$

where h_0 is the known distance from the sample datum surface to the plane of zero optical path difference. The depth range is therefore 0 to h_M where $h_M = z_M / 2$, and the depth resolution is $\delta h = \delta z / 2$.

3. System design

3.1 Field of view

The doubly telecentric lens pair L_1, L_2 in the interferometer has magnification

$$m_{21} = f_2 / f_1, \tag{5}$$

where f_1 and f_2 are the respective focal lengths of the two lenses. In the current setup $f_1 = f_2 =$ 150 mm, giving unit magnification, so that a $5\times5\text{mm}^2$ MLA corresponds to a field of view of the same size on the object.

3.2 Sampling requirement of object's image at MLA

Integral Field Units designed for astronomy purposes require that no loss of optical bandwidth is accrued through the system, as it would compromise the resolving power of the fore optics, usually an expensive telescope. The object's image therefore has to be sampled so that no loss of spatial frequencies occurs. This corresponds to the case where nearly plane waves arrive at the lenslets, each of which produces a spot at the back focal plane of the MLA as in a Shack-Hartmann sensor. It can be shown that the Shannon sampling requirement implies at least 4.88 lenslets across the diameter of the Airy disk of the PSF of lens L_2 [9]. This happens when the numerical aperture of the light beam from lens 2, NA_2, satisfies the inequality

$$\mathrm{NA}_2 \le \frac{\lambda_c}{4p_x^{MLA}}, \tag{6}$$

where λ_c is the centre wavelength and p_x^{MLA} is the separation of the lenslet centres along the x axis of the microlens array. NA_2 is related in turn to the diameter D_1 of the aperture stop E_1 given by

$$D_1 = 2f_2\mathrm{NA}_2. \tag{7}$$

It is worth pointing out that under this sampling condition a given point on the sample contributes signal to several lenslets. Therefore, although the sampling pitch on the sample is p_x^{MLA}/m_{21} (0.1 mm in our system), the true lateral resolution as defined by the Rayleigh resolution criterion is given by 2.44 p_x^{MLA}/m_{21} (0.244 mm). In certain cases, for example to increase the system's light throughput, it may be desirable to increase D_1 such that inequality (6) is no longer satisfied. If the object has a smoothly-varying specularly-reflecting surface, increasing D_1 increases the maximum surface slope of the object from which light is still passed by E_1. The light falling on each MLA is then tilted but still locally planar so the pupil plane spot location is shifted, but its size is unaffected. On the other hand, if the object has an optically rough surface, a speckle field then fills pupil E_1. The fact that the pupil plane spots are images of E_1 means that enlarging E_1 would cause each of the 'clean' spots in the pupils' plane to enlarge and become speckled, leading in turn to unwanted modulation of the 1-D intensity signals in the plane of the PDA, and also crosstalk between spectra.

The effective numerical aperture of lens L_1 is given by $NA_1=NA_2f_1/f_2$. NA_1 sets an upper limit to the surface slope of the object, defined by $\theta = \sin^{-1}(\mathrm{NA}_1)/2$, that can reflect light into the aperture of L_1 when a collimated beam illuminates the object. There is thus a fundamental trade-off between the maximum measurable surface slope and the field of view, the latter being proportional to f_1. Even though such limitations occur with all microscope-based metrology systems including SWLI, the constraint is more severe here for typical microlens array geometries because the NA is limited by the pitch of the lenslets through inequality (6).

3.3 MLA pupil plane

The MLA effective focal length, f_3, defines the position of the pupil plane. Each lenslet focuses light onto a spot with diameter

$$d_{PSF3} = 1.22\lambda_c / \mathrm{NA}_3. \tag{8}$$

In our system, however, the spot diameter is larger than the value predicted by Eq. (8). The size of the images on the PDA implies d_{PSF3}~10 μm, which is likely to be due to spherical and chromatic aberrations in the lenslets. This corresponds to an effective value NA_3 ~ 0.1 which we use hereafter.

3.4 Constraints on the size of the point spread functions

The spots on the MLA pupil plane are imaged by lens pair L_4, L_5 onto the PDA array with magnification m_{54}. Loss-less sampling requires at least 4.88 PDA pixels across the diameter of the imaged spots, i.e.

$$d_{PSF5} \geq 4.88 p_x^{PDA}, \tag{9}$$

with p_x^{PDA} the PDA pixel separation along the local x-axis ($p_x^{PDA} = p_y^{PDA}$ = 9 μm in the Apogee U16M). The minimum value of m_{54} (= $m_{54}^{\min}$) required to adequately sample the imaged spots can be determined from the fact that d_{PSF5}, the diameter of the point spread function on the plane of the PDA, equals $m_{54} d_{PSF3}$. From this,

$$m_{54}^{\min} = 4.88 p_x^{PDA} / d_{PSF3}. \tag{10}$$

$m_{54}^{\min}$ = 4.4 in the current system. The required number of pixels N_x^{PDA} along one edge of the PDA array is given by

$$N_x^{PDA} = 4.88 L_x^{MLA} / d_{PSF3}, \tag{11}$$

where L_x^{MLA} is the physical dimension of the MLA along the equivalent axis. For the current system a 5×5 mm^2 MLA is imaged onto ~2400×2400 pixels if a monochromatic source is used, and a slightly smaller MLA if broadband light is used, to allow for the spatial extent of the spectra.

3.5 Spatial arrangement of spectra on the PDA

The ratio between the MLA pitch and the diameter of the pupils,

$$R = p_x^{MLA} / d_{PSF3}, \tag{12}$$

is an important parameter linked to the number of 1-D spectra that can be packed onto the PDA. The larger the ratio, the more and longer the spectra that can be arranged without overlap. This requires lenslets with high NA. In the current MLA, the maximum achievable ratio would be $R \approx 100$ μm/10 μm = 10 provided that inequality (6) is satisfied. Disregarding the ring (after first zero) around the PSF central peak, this ratio means that up to 10 spectra could be tightly accommodated within the pitch of the microlens centre locations through appropriate choice of rotation angle α. In the current system α was chosen to be approximately 7˚, which reduces the number of spectra between adjacent spots in the vertical direction on the PDA to an effective value R = 7. This leaves bigger vertical gaps between the spectra to reduce crosstalk, as suggested in [8]. The maximum available length of a given spectrum on the PDA, so as to avoid overlap with neighboring ones along the grating dispersion direction, is approximately

$$l_s^{PDA} = p_x^{MLA} m_{54} (R+1), \tag{13}$$

where the effective value of R should be used.

3.6 NA of relay lenses in the hyperspectral imager

The aperture diameter, D_4, and focal length, f_4, required for lens L_4 must satisfy $D_4 \geq 2f_4\mathrm{NA}_3$ to capture the full cone of light emerging from the lenslets in the MLA. The lenslet array diagonal size, 5mm×√2, also needs to be accounted for to avoid vignetting, leading to a minimum required aperture stop diameter D_4~15 mm. In practice a somewhat larger value is preferable to allow the full cone of light to be captured from the outer lenslets. This is satisfied by an off-the-shelf NIR achromat with f_4 = 40 mm and diameter D_4 = 25 mm. Focal lengths f_5 = 150 mm and f_4 = 40 mm lead to an effective magnification $m_{54} = f_5/f_4 = 3.75$. The diameter of L_5 must match the diagonal of the image of the MLA on the PDA to reduce vignetting. Through Eq. (13) the values p_x^{MLA} = 0.1 mm, R = 7 and m_{54} = 3.75 lead to l_s^{PDA} = 3 mm, or ~333 pixels available on the PDA for each spectrum along the grating dispersion direction.

3.7 Diffraction grating

The relationship between the first order diffraction angle β_d of the rays originating from lenslet (m, n) and wavelength λ is given by the grating equation:

$$\sin\beta_d = \lambda F - \sin\beta_i, \tag{14}$$

where F is the grating frequency in lines mm^{-1}, β_i is the angle of incidence of the broadband collimated beam that reaches the grating from the lenslet and is defined by

$$\beta_i = \tan^{-1}\left(\frac{x^{MLA}}{f_4}\right), \tag{15}$$

where x^{MLA} is the x-coordinate of the relevant lenslet in the MLA's coordinate system and f_4 is the focal length of L_4.

The wavelength reflected back by FBG_1 can be taken as the reference wavelength, and the point at which it falls on the PDA array as the origin of a local coordinate system $(x_{m,n}^{PDA}, y_{m,n}^{PDA})$ for lenslet (m, n). The light at other wavelengths will therefore fall at position

$$x_{m,n}^{PDA}(\lambda) = f_5 \tan\left\{\sin^{-1}\left[\lambda F - \sin\beta_i\right] - \sin^{-1}\left[\lambda_1 F - \sin\beta_i\right]\right\}. \tag{16}$$

The required grating frequency is dependent both on the available length l_s^{PDA} given by Eq. (13), and on the bandwidth of the light source. It was noted above that an upper limit l_s^{PDA} = 3.0 mm would be available on the PDA to sample each of the spectra along the dispersion direction of the grating. It can be shown that an off-the-shelf grating with 300 lines/mm produces an angle between the diffracted orders for 815 nm and 865 nm given by $\Delta\beta = 0.0155$ rad (taking β_i=0) that corresponds to an effective spectrum length $l_s^{PDA*} = f_5 \times \Delta\beta = 2.32$ mm (or 258 pixels) on the PDA, about ~80% of the maximum available l_s^{PDA}. Off-axis incidence on the grating from micro lenses at the edges leads to values within 1.6% of the on-axis ones.

The surface position is extracted by finding the peak of the Fourier transform of the spectral fringes. A broad spectral range thus results in a narrow peak and better depth resolution than a narrower spectral range. However, increasing the bandwidth requires either a shorter focal length f_5 or lower grating frequency for the full spectrum to cover the same number of pixels in the PDA array, thus leading to larger δk, and hence smaller unambiguous depth range by Eq. (2). There is therefore a fundamental trade-off between depth resolution and unambiguous depth range.

4. Data reduction

In addition to an image of the interferogram, it is convenient to record two additional spectral images: one with the reference beam only (object beam blocked) and one with the object

beam only (reference beam blocked). These are needed only for the estimation of background intensity distribution; if true single-shot imaging is required, the background can be estimated by suitable scaling of the SLED spectrum for example as provided by a single measurement of the 'reference-beam-only' image. Such an approach may result in low frequency artefacts in the Fourier reconstruction of optical path difference, if the sample reflectivity varies strongly with wavelength, due to the resulting differences in the shape of the object beam and reference beam spectra. This region of the reconstruction can however be avoided simply by ensuring there is a sufficiently large offset between the reference and object optical path lengths.

The procedure to obtain a surface height map from the image of the spectra produced from the MLA pupils consists of the following steps, which are performed for all spectra in the image:

1. Find the coordinates $(x_{m,n}^{PDA\,1}, y_{m,n}^{PDA\,1})$ and $(x_{m,n}^{PDA\,2}, y_{m,n}^{PDA\,2})$ of the points where the reference wavelengths λ_1 and λ_2 fall on the PDA array when the 'Two wavelengths' illumination configuration is used (see Fig. 3). This is performed for all (m, n) with sub-pixel resolution by fitting a 2-D Gaussian function to each Airy disk.
2. Evaluate the distance, $d(m, n)$, between points $(x_{m,n}^{PDA\,1}, y_{m,n}^{PDA\,1})$ and $(x_{m,n}^{PDA\,2}, y_{m,n}^{PDA\,2})$, and the orientation (angle subtended to the PDA rows) of the line that connects them.
3. Use the distance $d(m, n)$ to scale the spectrum and find the wavelength for all other points along the spectrum. A linear relationship between position and wavelength is assumed, as the residuals relative to Eq. (16) do not exceed 0.08 of a pixel between 815 nm and 865 nm.
4. Evaluate pixel coordinates along the wavelength axis of the spectrum so that it can be re-sampled with equal steps along the wavenumber axis.
5. Interpolate the spectral interferogram, the reference beam spectrum and the object beam spectrum at the pixel coordinates found in step (4).
6. Remove the background intensity, or dc term, by subtracting the reference and object spectra from the spectral interferogram [6].
7. Multiply the re-sampled, dc-free 1-D intensity signal obtained in step (6) by a Hanning window to reduce phase noise due to crosstalk and then evaluate its Fourier transform.
8. Find the frequency at the maximum of the magnitude of the Fourier transform, which localizes the surface relative to a datum defined by the reference mirror in Fig. 1. This is done with sub-pixel resolution using the continuous Fourier transform [10].
9. Convert the peak frequency into OPD using the following relationship:

$$z = f_k \frac{2\pi}{\Delta k}, \tag{17}$$

   where f_k is the frequency in units of cycles across the spectral bandwidth used, Δk.
10. Convert OPD into surface height using Eq. (4).

5. Experimental results

A magnified portion of an image produced by the 'two wavelengths' configuration is shown in Fig. 3. The pattern corresponds to a square lattice with two bright spots at wavelengths λ_1

and λ_2 being produced from each pupil in the focal plane of the MLA. Some spectral power can be observed at intermediate wavelengths, i.e. along the straight line connecting both spots in the unit cells, due to an effective extinction ratio of ~1:70 for the fibre Bragg gratings and reflection at the single mode fibre end.

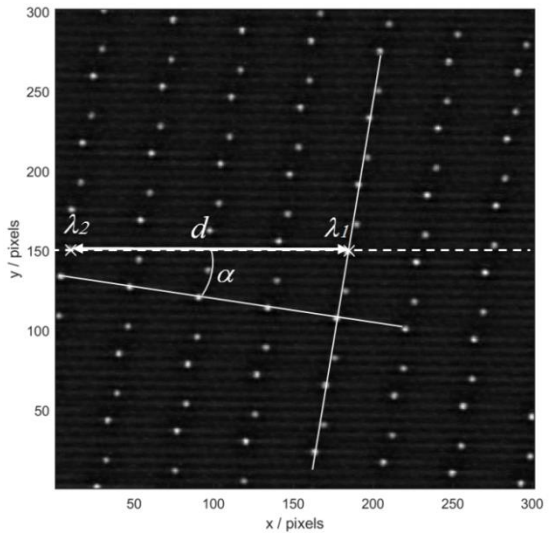

Fig. 3. Close-up of the spectra corresponding to the focal spots of the microlens array in the 'two wavelengths' configuration. The two crosses indicate the position of the λ_1 and λ_2 peaks from a single pupil, which are separated by a distance *d* on the PDA.

Figure 4 shows the distance, *d* (in pixels), between the centres of the peaks for λ_1 and λ_2 in the two wavelength configuration for a set of 35×35 lenslets. In an ideal optical system this distance should be the same for all spectra. However, lens distortions and non-linearity of the grating equation lead to a spatial variation across the PDA, which means that each spectrum has to be treated individually when position on the PDA is converted to wavenumber.

A magnified portion of an image produced by the 'broadband' configuration is shown in Fig. 5. Each horizontal 1-D interference signal is modulated with a spatial frequency that is proportional to the optical path difference between the reference mirror and the object surface imaged onto each lenslet, as explained in section 3. In this case, the dc term of the interference signal has been removed as described in Step 6 of section 4.

Figure 6(a) shows a horizontal profile along the middle of the unit cell in Fig. 5, between 810 nm and 835 nm but expressed here in terms of wavenumber. This is a spectral interferogram resulting from Step 7 of section 4 in which spatial frequency encodes optical path difference between the reference and the object at the point imaged by the corresponding lenslet in the microlens array. The modulation drops to values close to zero outside the range $k = 7.54 - 7.74 \times 10^6$ m^{-1}, corresponding to an effective wavelength range between 812 nm and 833 nm, which is less than half the specified bandwidth of the SLD source. The low modulation elsewhere in the spectrum is believed to be due to interference between front and back surfaces of the pellicle beam splitter (BS in Fig. 1) which leads to reduced spectral power of the reference and object beams for certain wavelengths. Figure 6(b) shows the magnitude of the Fourier transform of the signal in Fig. 6(a). The peak position is found between the integer frequency values produced by a discrete (fast) Fourier transform, by using an algorithm based on the continuous Fourier transform [10]. The continuous trace of

the transform from which the peak is extracted is shown with a continuous line and the position of the peak is indicated with a vertical line.

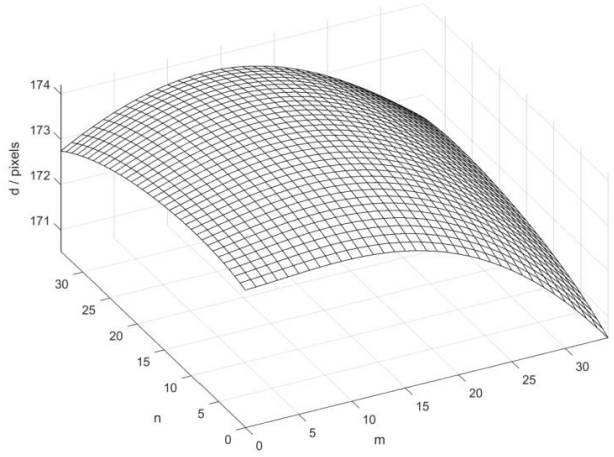

Fig. 4. Spatial distribution of the distance *d* between the λ_1 and λ_2 peak locations in the spectra.

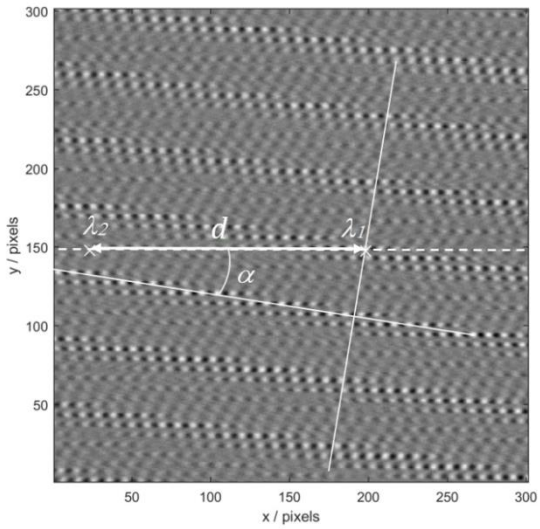

Fig. 5. Close-up of the 1-D horizontal interference patterns produced by dispersion of the focal spots of the microlens array when 'broadband' illumination is used. The dc term of the interference signal has been removed, so mid grey represents zero while darker and brighter levels represent negative and positive values, respectively.

In comparison with our previous HSI system [6, 7], a much higher pixel utilisation rate is achieved because the spectra are distributed across the PDA rather than within a horizontal band less than 20 pixels high. A 100% utilisation rate is not possible because some space

between spectra is required to avoid spectral crosstalk. Also the rotation of the MLA array relative to the PDA pixel array leads to some pixel loss. The fraction of pixels containing useful signal can be estimated from an image of the object beam alone by counting the pixels with intensity greater than a threshold given by a local average. In the current system, this leads to a utilisation rate of ~45%.

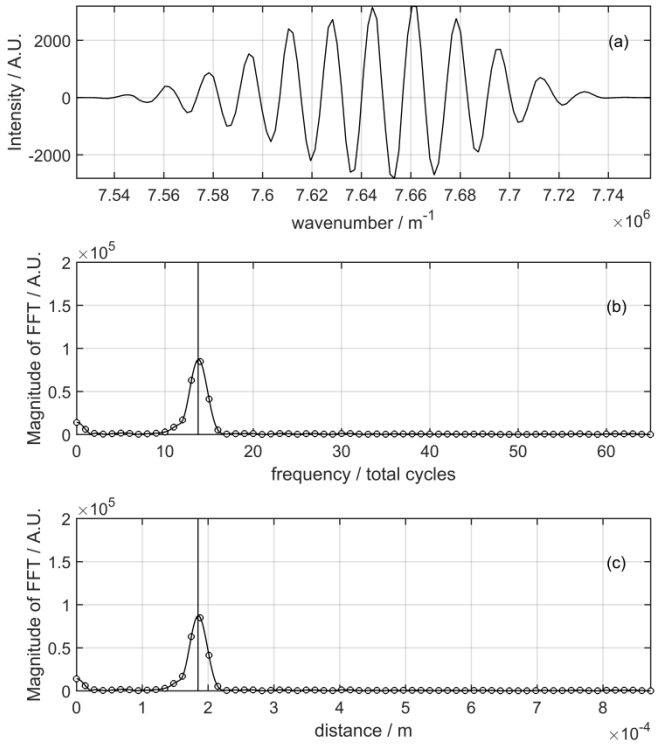

Fig. 6. Spectral interference profile for one lenslet after removal of the dc component: a) intensity signal; b) Fourier Transform of (a) (output of Fast Fourier Transform algorithm shown as open circles, with the continuous Fourier transform overlaid as a continuous line), from which the peak position (vertical line) is evaluated; c) as (b) but after scaling frequency to distance.

5.1 Flat surface

Figure 7 shows the 35×35 point surface profiles obtained when a flat mirror was used as the object and was shifted along the optical axis in steps of 50 μm ± 2 μm. 3675 independent coordinates were therefore measured. The mean displacement between the top and middle and middle and bottom measured profiles was 48.80 μm and 48.82 μm, respectively. The field of view on the object corresponds to 3.5 mm × 3.5 mm and the lateral resolution to 0.244 mm (see section 3.2). The spectral range 810-835 nm was effectively sampled with 131 pixels, i.e. $\delta\lambda$ = 0.19 nm, and $\delta k = 1.77\times10^3$ m^{-1}, which corresponds to a depth range $h_M = \pi/2\delta k$ = 0.88 mm.

An rms value of 0.49 μm was obtained for the height data after subtracting second order terms that arise due to lens distortions. In profilometry, the height measurement accuracy is usually expressed as the surface position uncertainty relative to the height measurement range, rms/h_M, with rms the root mean square deviation of the measurement relative to the

true figure. This ratio defines the inverse of the 'dynamic range'. In this system, they are equal to 5.3×10^{-4} and 1871, respectively.

A small ripple is however observed on each surface reconstruction. The rms deviation about best fit planes of the top, middle and bottom surface profiles was 0.725 μm, 0.619 μm and 0.556 μm, respectively, which is significantly higher than the known flatness of the mirror (λ/10 @ 633 nm). A correlation was found between this ripple and the spatial variation of the size of the Airy discs at the pupil plane of the MLA. Figure 8(a) shows the residual of the height $h(x, y)$ shown as the top mesh in Fig. 7 with respect to a linear fit. Figures 8(b) and 8(c) show the spatial variation of the horizontal and vertical extent of the spots corresponding to λ_2 imaged at the PDA when the reference arm is blocked and the 'two wavelengths' configuration is used. These correspond to the standard deviations of a 2D-Gaussian best fit in the horizontal and vertical directions. One possibility is that the ripple is caused by variations in the focal length of the lenslets, which would lead to systematic spatial variations in cross talk between channels. The manufacturer's claimed error in the radius of curvature of the lenses is however relatively small (less than 1% over a $5\times5mm^2$ MLA). It seems plausible that this variation in spot size could feed into a corresponding spatial variation of cross-talk between channels. It is worth pointing out that spherical and coma aberrations of double achromats L_4 and L_5 increase for off axis incidence and thus affect the pupil spots of microlenses around the edge of the array. Their effect is to distort and enlarge their image on the PDA, leading to increased crosstalk (overlap between neighbouring spectra). A straightforward improvement would be to replace the double achromats by better corrected lenses, which may allow imaging the full extent of the MLA.

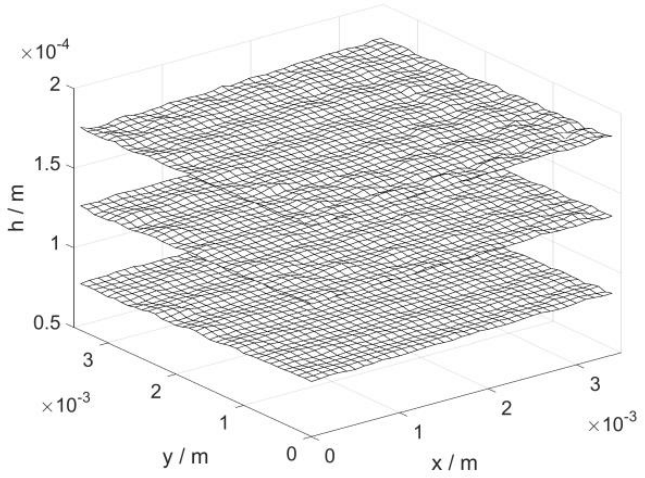

Fig. 7. Three surface height measurements of a flat mirror with normal shifts of 50 μm.

5.2 Surface step

An example of a discontinuous surface is shown in Fig. 9, which is the measured height map of a circular microscope cover slip placed on a glass substrate. Again 35×35 lenslets of the full MLA were used to acquire the data. Clean transitions are observed at the edge of the step. The height of the step as measured from the data is 108.7 μm.

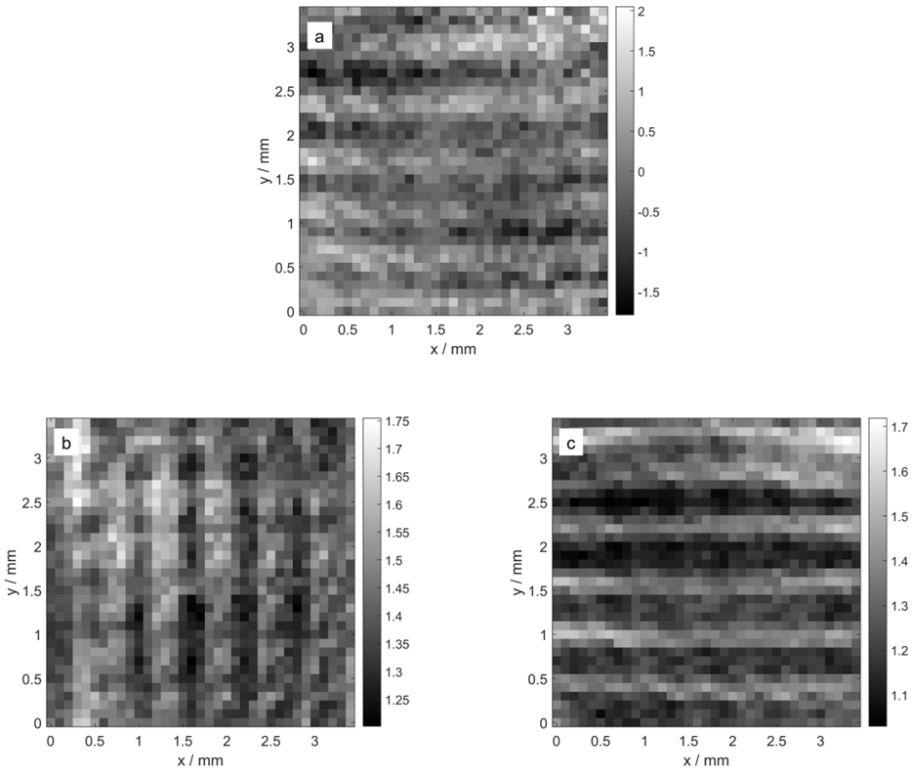

Fig. 8. (a) Residual of the height map $h(x, y)$ shown at the top in Fig.(7) with respect to a linear fit (in μm). (b) and (c) show, respectively, the spatial variation of the horizontal and vertical extent (measured in pixels) of the spots corresponding to λ_2 imaged at the PDA when the reference arm is blocked. These correspond to the standard deviations of a 2D-Gaussian best fit in the horizontal and vertical directions.

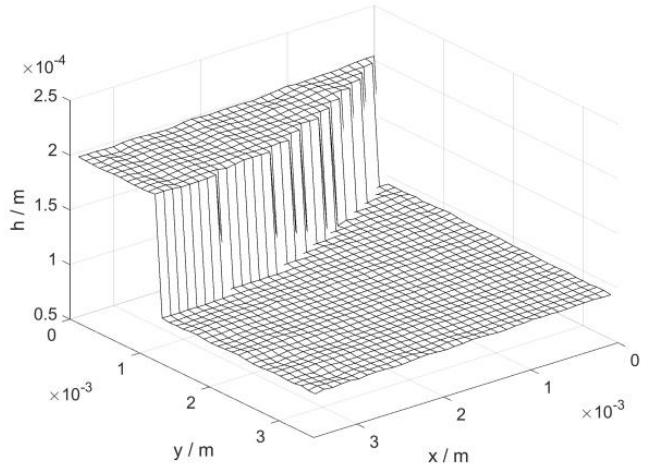

Fig. 9. Surface profile of the edge of a circular microscope cover slip on a glass substrate measured using 35×35 lenslets of the MLA.

6. Conclusions

A hyperspectral interferometry system able to measure surface form on a grid of points in a single shot has been developed and presented in this paper. No mechanical scanning mechanism is needed, unlike the positioning stage used in SWLI or tunable wavelength selection device in WSI. The approach is thus applicable to moving objects given a sufficiently short duration pulsed light source.

The optical configuration presented here, which is based on a microlens array, uses significantly more of the pixels from a square or rectangular format image sensor than do previously reported systems (>40% instead of ~2%), with consequent benefits to the number of measured coordinates and/or the measurable depth range.

The setup also avoids the need for the etalon used in previous systems and thus has significantly improved light efficiency. One limitation of the approach is that changes in surface slope have the effect of shifting the spectra on the photodetector array, eventually leading to cross talk between channels. An array of 35×35 independent points was measured simultaneously in a square grid with a pitch of 100 μm, covering a FOV of 3.5×3.5 mm^2 and with a depth range of 880 μm. The system was tested with specular surfaces and achieved an *rms* height error of 0.49 μm for a flat mirror, mainly dependent on lens aberrations which affect in particular the off-axis spectra.

Funding

The Royal Society (Industry Fellowship IF2012/R2) and the Engineering and Physical Sciences Research Council (EP/K018124/1).

Acknowledgments

P. D. Ruiz acknowledges The Royal Society and industrial hosts Phase Vision Ltd. and Renishaw plc for their support.